Journal of Materials Chemistry B

Accepted Manuscript

ROYAL SOCIETY OF CHEMISTRY

www.rsc.org/materialsB

Co-delivery of camptothecin and curcumin by cationic polymeric nanoparticles for synergistic colon cancer combination chemotherapy†

Bo Xiao[a,b]*, Xiaoying Si[a], Moon Kwon Han[b], Emilie Viennois[b,c], Mingzhen Zhang[b], Didier Merlin[b,c]

Abstract

Nanoparticle (NP)-based combination chemotherapy has been proposed as a potent strategy for enhancing intracellular drug concentrations and achieving synergistic effects in colon cancer therapy. Here, we fabricated a series of chitosan-functionalized camptothecin (CPT)/curcumin (CUR)-loaded polymeric NPs with various weight ratios of CPT to CUR. The resultant cationic spherical CPT/CUR-NPs had a desirable particle size (193–224 nm), relatively narrow size distribution, and slightly positive zeta-potential. These NPs exhibited a simultaneous sustained release profile for both drugs throughout the study period with a slight, initial burst release. Subsequent cellular uptake experiments demonstrated that the introduction of chitosan to the NP surface markedly increased cellular-uptake efficiency compared with other drug formulations, and thus increased the intracellular drug concentrations. Importantly, the combined delivery of CPT and CUR in a single NP enhanced synergistic effects of the two drugs. Among the five cationic CPT/CUR-NPs tested, NPs with a CPT/CUR weight ratio of 4:1 showed the highest anticancer activity, resulting in a combination index of approximately 0.46. In summary, our study represents the first report of combinational application of CPT and CUR with a one-step–fabricated co-delivery system for effective colon cancer combination chemotherapy.

1. Introduction

Colon cancer, the third-most common malignant tumor, is associated with high mortality, accounting for more than 1.4 million new cases and over half a million deaths worldwide annually [1, 2]. Current therapeutic approaches for colon cancer treatment include surgery, chemotherapy, and radiotherapy. Of these modalities, chemotherapy is the most effective method [3]. However, application of a single chemotherapeutic agent often fails to achieve complete cancer remission owing to the heterogeneity of cancer cells, development of drug resistance, and adverse effects caused by high and/or repeated drug dosing [4-6]. To overcome these issues, clinicians have adopted combination chemotherapy based on multiple chemotherapeutic drugs as a primary cancer treatment regimen [7]. It has been reported that the use of multiple drugs targeting different cellular pathways can raise the genetic barriers for cancer cell mutations, and thus delay the cancer adaptation process [8-10]. Moreover, simultaneous administration of multiple drugs provides synergistic antitumor efficacy [11].

Camptothecin (CPT), a hydrophobic plant alkaloid extracted from *Camptotheca acuminate*, exhibits a broad spectrum of antitumor activity against various cancers, including colon cancer, small cell lung carcinoma, and breast cancer [12]. Mechanistically, CPT converts the DNA unwinding/winding enzyme topoisomerase I into a cellular poison by inhibiting the religation step through stabilization of the DNA/topoisomerase I complex and formation of a cleavable DNA/enzyme/CPT ternary complex. Following collision of the replication fork with this cleaved strand of DNA, the cell cycle arrests in the G2 phase, thus inducing cell death [13, 14]. Although CPT has been proven to possess impressive preclinical antitumor activities, its clinical application has been seriously restricted by limited efficacy and dose-limiting toxicity. Therefore, CPT is often utilized in combination with other drugs [10, 15, 16]. Curcumin (CUR), a hydrophobic polyphenol derived from natural herbal sources, has a

variety of therapeutic properties, including antioxidant, anti-inflammatory, and antitumor activities [17, 18]. Recently, CUR has received increasing attention for cancer therapy due to its unique beneficial features, including (1) relative safety for humans, even when given at a high doses (12 g/d) for 3 months; (2) inhibition of various cellular pathways associated with tumor survival and progression; and (3) suppression of chemoresistance through sensitization of cancer cells to conventional chemotherapeutic agents [19-21]. Accordingly, synergistic effects of CUR and various anticancer agents have been previously explored. Scarano *et al.* reported that CUR potentiates the effects of platinum, with a combination index (CI) reflective of synergy ranging from 0.4 to 0.8 [17]. Also, Ganta *et al.* demonstrated that the combination of CUR and paclitaxel was very effective in enhancing cytotoxicity towards cancer cells by promoting an apoptotic response [22]. Hence, considering the different antitumor mechanisms of CPT and CUR, the combination of these two drugs might offer a viable therapeutic option for cancer treatment.

As reported previously, the clinical outcome of combination chemotherapy is highly dependent on the ratio of administrated drugs, which in turn determines the level of synergism or antagonism [8]. Another challenge for combination chemotherapy is unifying the pharmacokinetics and cellular uptake of various drugs [15, 23, 24]. Notably, combinational nanoparticles (NPs) provide an excellent platform for overcoming these challenges owing to their simultaneous delivery of the correct ratio of drugs to individual cells, synergistic therapeutic effects, and suppression of drug resistance [25-27]. The choice of carrier material is highly important since it significantly affects the pharmacokinetics and pharmacodynamics of drugs. To date, a wide range of polymers, including lipids, poly(lactic acid/glycolic acid) (PLGA) and dendrimers, have been employed as drug carriers [28-30]. Among these, PLGA is a FDA-approved biodegradable copolymer that can encapsulate

hydrophobic drugs to form NPs with high efficiency. Accordingly, it has been widely used in drug delivery [31, 32]. Unfortunately, the negative surface charge of PLGA NPs tends to impair their interaction with the cell surface, leading to low cellular internalization [33]. Generally, the physicochemical characteristics of NPs, such as particle size, surface charge, composition and surface hydrophobicity, affect their cellular uptake [34]. Of these characteristics, surface charge is the factor that exerts the greatest influence on drug-delivery function [35]. It has been reported that cationic NPs can easily bind to the negatively charged cell membrane, facilitating cellular uptake and intracellular drug release [33]. Chitosan, a cationic biodegradable polymer, provides a strong electrical interaction with the negative-charged NPs surface, switching the surface to a positive charge [36-38]. In our previous report, we optimized the parameters for preparing chitosan-functionalized NPs, and also confirmed that chitosan functionalization increases the cellular uptake and tumor accumulation of NPs [30].

In the present study, using chitosan as a material for surface functionalization of NPs, we describe the first attempt to fabricate cationic CPT/CUR-loaded PLGA polymeric NPs, as depicted in Figure 1a. Subsequently, we characterized their physicochemical, including hydrodynamic particle size, zeta-potential, drug loading and encapsulation efficiency, and further evaluated their cellular uptake efficiency. We also assessed the antitumor synergistic effects of cationic CPT/CUR-loaded PLGA polymeric NPs *in vitro*.

2. Materials and Methods

2.1.Materials

PLGA (Mw = 38–54 kg/mol), poly(vinyl alcohol) (PVA, 86-89% hydrolyzed, low molecular weight), chitosan, sodium nitrite, CPT, CUR, accutase and Triton X-100 were purchased from Sigma-Aldrich (St. Louis, MO, USA). Paraformaldehyde stock solution (16%) was from Electron Microscopy Science (Hatfield, PA, USA). Vybrant® MTT cell proliferation assay kit was supplied from Invitrogen (Eugene, OR, USA). All commercial products were used without further purification.

2.2. Depolymerization of chitosan and intrinsic viscosity measurement

Molecular weight of chitosan was tailored by depolymerization using sodium nitrite following a reported method [39]. Viscosity-average molecular weight of the resulting chitosan was determined as 1.8×10^4 using a 0.5 M CH_3COOH/0.2 M CH_3COONa by viscometric method [40]. The depolymerized chitosan was used in the NPs fabrication process.

2.3. Fabrication of NPs

NPs were prepared by a modified oil-in-water (O/W) emulsion-solvent evaporation technique. Briefly, 100 mg of PLGA and, optionally, various amounts of CPT and CUR (total 6 mg) were co-dissolved in 2 mL of dichloromethane (DCM)-methanol co-solvent (8:2). The resulting organic solution was added drop-wise to 4 mL PVA solutions (5%) with or without depolymerized chitosan (0.5%). Subsequently, the mixture was sonicated six times (10 s each time) at 50% amplitude in an ice bath using a Sonifier 450 (Branson Sonic Power, Danbury, CT, USA). This emulsion was immediately poured into 100 mL of aqueous solution containing 0.3% PVA with or without 0.03% depolymerized chitosan. After that, the organic solvent was evaporated under low vacuum conditions (Rotary evaporator, Yamato RE200,

Santa Clara, CA, USA). The NPs formed by this method were collected by centrifugation at 12,000 g for 20 min, washed three times with deionized water, dried in a lyophilizer, and stored at –20 ^{o}C in airtight container. The resultant chitosan-functionalized CPT/CUR-loaded NPs were named as cationic CPT/CUR-NPs (i) (i = 1:4, 1:2, 1:1, 2:1 and 4:1), and the feed weight ratio of CPT/CUR were denoted by the numbers in bracketed text.

2.4 Characterization of NPs

Particle sizes (nm), size distribution and zeta-potential (mV) of NPs were measured by dynamic light scattering (DLS) using 90 Plus/BI-MAS (Multi-angle particle sizing) or DLS after applying an electric field using a ZetaPlus (Zeta potential analyzer, Brookhaven Instruments Corporation, Holtsville, NY, USA). The average and standard deviations of the diameters (nm) or zeta-potential (mV) were calculated using 3 runs. Each run is an average of 10 measurements.

The morphology of NPs was observed with a transmission electron microscope (TEM, LEO 906E, Zeiss, Germany). A drop of dilute NPs suspension was mounted onto 400-mesh carbon-coated copper grids and dried before analysis.

UV-vis absorption spectra of CPT and CUR were obtained on a Shimadzu UV-1700 UV/Vis spectrophotometer. The absorption intensity of CUR was measured at 435 nm. Fluorescence spectra of CPT and CUR were recorded on a Shimadzu RF-5301 PC spectrofluorometer. The fluorescence intensity of CPT was measured at 435 nm emission wavelength (360 nm excitation wavelength). Quartz cuvettes were used in all UV and fluorescent studies. The amount of CPT and CUR encapsulated in NPs was determined by measuring the intrinsic fluorescence of CPT and adsorption of CUR, respectively. In a typical example, NPs (2 mg) were dissolved in 1 mL of dimethyl sulfoxide (DMSO). Then the supernatant was diluted and transferred to quartz cuvette for measurement.

XRD spectra were examined using a Cu Ka-ray with tube conditions of 40 kV and 30 mA ranging from 10^o to 50^o (XRD-7000, Shimadzu, Japan).

2.5 Release profiles of CPT and CUR from NPs

The release behaviour of CPT and CUR from NPs was conducted by the dialysis method as described in our group before [30]. Briefly, NPs were dispersed in PBS to form a suspension (equal to 200 μg of drug). The suspension was transferred into a regenerated Cellulose Dialysis tube (molecular weight cut-off = 10,000 Da) and the sample-filled tube was closed tightly at both ends to keep each tube surface area equivalent. The closed bag was subsequently put into a centrifuge tube, and immersed in 20 mL PBS release medium containing 0.5% Tween-80. Tween-80 was employed in PBS to maintain the solubility of drugs in aqueous phase. The tube was put in a water bath shaking at 100 rpm at 37 ^{o}C for 72 h. At appropriate time points, outer solution was taken for measurement and fresh release medium was added. The amount of CPT and CUR in the outer solution was measured according to the method described in Section 2.4. All of the operations were carried out in triplicate.

2.6 Intracellular NPs uptake visualization

Colon-26 cells were seeded in eight-chamber tissue culture glass slide (BD Falcon, Bedford, MA, USA) at a density of 5.0×10^4 cells/well and incubated overnight. The culture medium was exchanged to serum-free medium containing cationic CPT/CUR-NPs (1:1). The total drug concentration in the medium is set as 100 μM. After 3 h of co-culture, the cells were thoroughly rinsed with cold PBS for 3 times to eliminate excess of NPs, and then fixed in 4% paraformaldehyde for 15 min. Images were acquired using an Olympus equipped with a Hamamatsu Digital Camera ORCA-03G.

2.7 Quantification of cellular uptake using flow cytometry (FCM)

Colon-26 cells were seeded in 6-well plates at a density of 3×10^5 cells/well and incubated overnight. The medium was exchanged to serum-free medium containing free CPT or various NPs (equal to 50 μM drug). Cells without treatment were used as negative controls. After 3 h of co-incubation, the cells were thoroughly rinsed with cold PBS to eliminate excess of NPs, which were not taken up by cells. Subsequently, the treated cells were harvested using accutase, transferred to centrifuge tubes, and centrifuged at 1,500 rpm for 5 min. Upon removal of the supernatant, the cells were re-suspended in 0.5 mL of FCM buffer, transferred to round-bottom polystyrene test tubes (BD Falcon, 12 × 75 mm), and kept at 4 ^{o}C until analysis. Analytical FCM was performed using the DAPI channel and FITC channel on the FCM Canto^{TM} (BD Biosciences, San Jose, CA, USA). A total of 5,000 ungated cells were analyzed.

2.8 MTT assay and synergy analysis

For 3-(4,5-Dimethylthiazol-2-yl)-2,5-Diphenyl Tetrazolium Bromide assay (MTT) test, Colon-26 cells were seeded at a density of 2×10^4 cells/well in 96-well plates and incubated overnight. The cells were incubated in the RPMI 1640 medium containing various amounts of drug (0 – 64 μM) for 24 h and 48 h, respectively. Free drug was dissolved in 9:1 (v/v) medium/DMSO, and NPs were suspended in medium. At the end of the incubation period, the cells were thoroughly rinsed three times with PBS. Cells were then incubated with MTT (0.5 mg/mL) at 37 °C for 4 h. Thereafter, the media were discarded and 50 μL DMSO was added to each well prior to spectrophotometric measurements at 570 nm. Untreated cells were used as negative references, whereas cells were treated with 0.5% Triton X-100 as positive controls.

CalcuSyn software (Biosoft, Cambridge, UK) was used to calculate the CI value. The CI values were determined at the half maximal (50%) toxicity concentration (IC_{50}). The

interaction between treatment modalities was calculated by using the median-effect equation and CI analysis. CI values of 0.9–1.1 indicate additive activity, values less than 0.9 indicate drug synergy, and values more than 1.1 indicate antagonism. CI analysis was performed by CalcuSyn software 1.0.

2.9 Quantitative reverse-transcription PCR (qRT-PCR)

Colon-26 cells were seeded in 6-well plates at a density of 5×10^5 cells/well and incubated overnight. Cationic CPT-NPs (CPT, 25 μM), cationic CUR-NPs (CUR, 25 μM) or cationic CPT/CUR-NPs (total drugs, 25 μM) were added to the medium. After 8 h of co-incubation, total RNA was extracted using the RNeasy Plus Mini Kit (Qiagen, Valencia, CA, USA). The complementary DNA (cDNA) was generated from the total RNAs isolated above using the Maxima First Strand cDNA Synthesis Kit (Fermentas, Hanover, MD, USA) according to the manufacturer's instructions. Levels of Bcl-2 RNA expression were quantified by reverse-transcription polymerase chain reaction using Maxima SYBR Green/ROX qPCR Master Mix (Fermentas, Hanover, MD, USA). The data were normalized to the internal control: 36B4. Relative gene expression levels were calculated using the $2^{-\Delta\Delta Ct}$ method. Sequences of all the primers used for reverse-transcription polymerase chain reaction are given in Table 3.

2.10 Electrical impedance sensing (ECIS) technology

Cell-attachment assays were performed to investigate the real-time cytotoxicity of NPs using electrical impedance sensing (ECIS) technology (Applied BioPhysics, Troy, NY, USA). The ECIS model 1600R was used for these experiments. The measurement system consists of an 8-well culture dish (ECIS 8W1E plate), the surface of which is seeded with Caco2-BBE cells at a density of 1×10^6/well. Once cells reached confluence, various NPs were added to the wells and the drug concentration in the medium is set as 25 μM. Untreated cells were used as negative references, whereas cells were treated with 0.5% Triton X-100 as positive controls.

Basal resistance measurements were performed using the ideal frequency for Caco2-BBE cells, 500 Hz, and a voltage of 1 V.

2.11 Statistical analysis

Statistical analysis was performed using Student′s *t*-test. Data were expressed as mean ± standard error of mean (S.E.M.). Statistical significance was represented by $*P<0.05$ and $**P<0.01$.

3 Results and discussion

3.1. Fabrication of NPs

We prepared various NPs using the emulsion-solvent evaporation technique, a common and well-established method for fabricating active-substance–loaded NPs [41]. Theoretically, rapid addition of the organic phase (PLGA; optionally CPT/CUR) to the aqueous phase together with an emulsifier (PVA; optionally chitosan), with sonication, leads to the immediate formation of an oil/water emulsion based on the Gibbs-Marangoni effect (mechanical mechanism) and a capillary break-up mechanism [42]. Upon evaporation of DCM/methanol co-solvents under reduced pressure, CPT/CUR molecules are transferred to the PLGA hydrophobic core through hydrophobic interactions (the "like dissolves like" principle) and further solidified to form compacted NPs [43].

Emulsifiers presented at the interface serve to separate oil and water phases, and are necessary to prevent aggregation of NPs [44]. PVA, a copolymer of hydrophobic poly(vinyl acetate) and hydrophilic poly(vinyl alcohol), is extensively utilized as an emulsifier for the fabrication of polyester NPs [45]. During the NP-formation process, the hydrophobic segments of PVA penetrate into the organic phase and remain entrapped in the polymeric matrix of the NPs; their hydrophilic segments surround NPs and stabilize them through steric hindrance. Chitosan is a natural, linear, cationic polymer that has long been used for surface modification of polyester NPs to prolong pharmacological effects [46, 47]. This action of chitosan coating could be attributable to the effects of chain entanglement with PVA. Alternatively, it may reflect adsorption of positively charged chitosan to the negative-charged NP surface.

3.2. Physicochemical characterization of NPs

Particle size and zeta-potential are critical parameters because they directly impact the stability, cellular uptake, and biodistribution of NPs [42]. As summarized in Table 1, DLS measurements showed that the average hydrodynamic diameter of NPs was in the range of 193 to 248 nm. The introduction of chitosan to the CPT-NPs surface produced no noticeable change in NP particle size. Interestingly, the particle size of all dual-drug–loaded NPs was much smaller than that of single-drug–loaded NPs, which might be contributed to its lower drug loading.

Generally, the charge on the NPs surface acts as an important factor that influences the stability of NP suspensions and the interaction between NPs and cell membrane. Table 1 also shows that NPs produced using PVA as an emulsifier were electronegative, whereas all chitosan-functionalized NPs had a positive zeta-potential (approximately +20 mV), reflecting the positive charge arising from the amino groups in chitosan units. Zeta-potential measurements suggested that the NPs as prepared were relatively stable and might also be favorable for delivering encapsulated drugs to cells owing to potential interactions between the positively charged NP surface and negatively charged cell membrane.

UV absorption intensity at 435 nm and fluorescence emission at 435 nm (excitation: 360 nm) of CPT and CUR do not overlap (ESI Fig. 1); thus, these parameters are suitable for use in quantifying CPT and CUR. Among prepared NPs, drug loading ranged from 2.1% to 5.8%, with the corresponding encapsulation efficiency depending on the drug type and the number of different drugs used in the fabrication process, as indicated in Table 1. For example, single-drug–loaded NPs exhibited high encapsulation efficiency, whereas the encapsulation efficiency of dual-drug–loaded NPs was markedly decreased.

As shown in Figure 1b, the size of cationic CPT/CUR-NPs (4:1) exhibited an approximate Gaussian distribution with a very narrow particle size distribution (polydispersity index,

0.18); the average size of NPs was ~209 nm. A representative transmission electron microscopy (TEM) image (Figure 1c) showed that these NPs are spherical with a mean diameter of approximately 138.5 nm. The modest deviation in diameter measured by DLS and TEM is attributable to differences in the surface states of the samples under the test conditions used, as reported in our previous studies [48]. Specifically, NPs were in a fully hydrated (swollen) state when tested by DLS, whereas they must be strictly dehydrated for TEM characterization. It has been proposed that most cells preferentially internalize slightly positively charged NPs with a size less than 400 nm [49-51]. On the other hand, to ensure efficient endocytosis, NPs should be large enough to prevent their rapid leakage into capillary blood vessels and capture by macrophages lodged in the reticuloendothelial system. The size of NPs was thus regulated in such a way that the mean size of NPs was larger than 100 nm, but smaller than 400 nm. Therefore, the properties of the cationic NPs described above would be considered favorable for internalization into cells.

To further elucidate the interactions between drugs and PLGA polymer, we investigated their X-ray diffraction (XRD) patterns. As shown in Figure 2, the representative XRD diffractograms of CPT and CUR showed numerous sharp and intense peaks at various scattering angles (2θ), reflecting their highly crystalline nature. In contrast, the XRD of cationic CPT/CUR-NPs (4:1) exhibited a complete absence of such characteristic peaks, possibly suggesting the formation of an amorphous complex upon intermolecular interaction between CPT/CUR and PLGA polymers. Thus, our results clearly indicate that the drugs were molecularly dispersed within the polymers, an observation in good agreement with a published report [8]. This is important because an amorphous drug prevents the Ostwald ripening phenomenon, which has a destabilizing effect.

3.3. In vitro drug-release profile

Controlled release of CPT and CUR from NPs is an important prerequisite for colon cancer therapy. *In vitro* release profiles of drugs loaded in cationic CPT/CUR-NPs (1:1) as a function of time are presented in Figure 3, which shows that approximately 15.5% and 47.6% of the initial dose of CPT was released from the polymeric matrix of the NPs during the first 4 and 24 h, respectively. The release rate of CUR within the first 4 h was faster than that of CPT, but slowly leveled off to lower values after 24 h. The differences in the release rates of CPT and CUR are likely attributable to differences in their hydrophobicity: because CPT is more water-soluble and readily diffuses into solution from the polymer matrix, it exhibits a faster release rate. We also found that CPT and CUR could be released simultaneously with a slight initial rapid release followed by a relatively slower release phase. As previously reported, drug release from PLGA NPs reflects the combined effects of swelling, pore diffusion, erosion, and degradation processes [52]. Accordingly, the initial burst release might be due to the diffusion of drugs present at the surface of NPs. Subsequently, drugs migrate from the core to the surface of the polymeric matrix, and show a moderate and sustained release behavior.

3.4. Intracellular uptake

Efficient cellular uptake is a major requirement for the therapeutic efficacy of NPs. Here, taking advantage of the intrinsic fluorescence of CPT and CUR, we investigated their intracellular delivery into cancer cells. Colon-26 cells were treated with cationic CPT/CUR-NPs (1:1) for 3 h. As shown in Figure 4, CPT and CUR fluorescence were clearly colocalized in Colon-26 cells, demonstrating that treatment with NPs resulted in drug accumulation in these cells.

To quantitatively assess the effect of NP encapsulation on cellular uptake of drug, we treated Colon-26 cells with free CPT (50 μM) or various NPs loaded with the same concentration of

CPT, and investigated their cellular uptake profiles after 3 h of co-incubation. The fluorescence emission intensities of Colon-26 cells treated with free CPT or various CPT-loaded NPs are presented in Figure 5a and 5b. Impressively, the fluorescence intensity of Colon-26 cells incubated with cationic CPT-loaded NPs was 2.1- and 2.8-fold higher than that of cells incubated with free CPT and CPT-loaded NPs, respectively. This indicates that surface modification with chitosan endows NPs with a greater ability to enhance cellular uptake efficiency, an observation in good agreement with our previous report [30]. We also incubated Colon-26 cells with empty NPs or cationic CPT/CUR-NPs (1:1). As can be seen in Figure 5c, CPT and CUR signals were simultaneously present in NP-treated cells clearly. This result confirms the colocalization of both drugs in the same cells, consistent with the results shown in Figure 4.

3.5. In vitro cytotoxicity and synergistic effect

To confirm the synergistic effect of CPT and CUR in drug-loaded NPs, we evaluated the *in vitro* cytotoxicity of the free drugs and various NPs using MTT assays. First, empty NPs were tested and shown to exert no obvious cytotoxicity on Colon-26 cells, even at a concentration up to 250 μg/mL (Figure 6a). Therefore, NPs without drugs were well tolerated by Colon-26 cells at this experimental concentration. To determine whether PLGA-encapsulated CPT/CUR maintain their anticancer activity, we investigated their effects on Colon-26 cells at different time points (24 and 48 h). As shown in Figure 6 (b and c) and Table 2, the anticancer activities of free drugs, cationic CPT-NPs and cationic CUR-NPs were dependent on their concentrations. Notably, whereas cationic CPT-NPs exerted much higher cytotoxicity toward Colon-26 cells than free CPT after 24 and 48 h of treatment, cationic CUR-NPs exhibited much lower cytotoxicity than free CUR. Four factors appear to account for these results: (1) the presence of DMSO in the free-drug solution assisted the

penetration of free drugs into cells; (2) DMSO itself exerted a toxic effect that was superimposed on that of free drugs; (3) CPT has much stronger cytotoxicity against Colon-26 cells than CUR; (4) cationic NPs deliver more drugs to cells than free drug formulation dissolved in DMSO. Furthermore, among the different treatments, cationic CPT-NPs exerted the strongest anticancer effects after 24 and 48 h of co-incubation. Using IC_{50} values of the individual drugs (Table 2), we investigated the synergistic effects of CPT and CUR at a fixed combined concentration of 8 μM. As indicated in Figure 6d, the synergistic efficacy of dual-drug combinations depends largely on the drug ratio and time interval. Figure 7 clearly indicates that a specific ratiometric combination was more powerful than a random combination of the two drugs. Strong synergism, reflected by CI values < 0.62, was evident at CPT/CUR ratios of 1:1, 2:1, and 4:1 after 24 h of incubation. A similar trend of ratio-dependent synergy was observed after 48 h of incubation, and strong synergism (CI < 0.46) was observed at a CPT/CUR ratio of 4:1. On the basis of these results, we selected cationic CPT/CUR-loaded NPs (4:1) for further study.

Bcl-2 regulates the mitochondria-mediated apoptosis pathway, and it has a dominant role in the survival of multiple malignancies [53]. Reducing its expression level is expected to promote apoptosis and therefore suppress the tumor cell growth. As shown in Figure 8a, Colon-26 cells had varied responses in Bcl-2 expression with the treatment of different NPs. Bcl-2 mRNA reduction following treatment with cationic CPT/CUR-NPs (4:1) was 58.8% compared to 43.7% following treatment with cationic CPT-NPs and 3.7% with cationic CUR-NPs. These results indicated that cationic CPT/CUR-NPs (4:1) exhibited pronounced effect on cell apoptosis, which was consistent with MTT data.

As indicated in a previous report, MTT assays are not suitable for real-time analysis of cellular transformation [54]. As an alternative, we employed ECIS, an automated, real-time

analytical tool for measuring cellular proliferation, cytotoxicity, and apoptosis [55]. As shown in Figure 8b, Caco2-BBE cells attached to the electrode surface to form a confluent monolayer with a resistance of approximately 32,000 Ohms. These cells were then incubated with various NPs containing the same drug concentration. Untreated Caco2-BBE monolayers exhibited a continuous increase in resistance, indicative of proliferation, whereas those treated with Triton X-100, used as a positive control (100% cell death), exhibited a sharp decrease in resistance. Interestingly, cationic NPs slightly increased resistance initially, followed by a subsequent decrease. This bimodal effect might indicate that the efficient controlled drug release behavior of NPs restricted the initial burst effect. Notably, cationic CPT/CUR-NPs (4:1) showed the lowest resistance, indicating that this NP formulation yielded the strongest anticancer activity among these three types of NPs.

3. Conclusions

In the present study, cationic PLGA NPs were employed as carriers to co-deliver CPT and CUR for colon cancer combination chemotherapy. The resultant NPs had desirable diameters and size distribution, and a slightly positive zeta-potential. Studies on drug release and cellular uptake of this co-delivery system showed that both drugs were effectively taken up by cells and released simultaneously. Cationic CPT/CUR-NPs exhibited clear synergistic effects against Colon-26 cells. Furthermore, these synergistic effects depended on drug ratios, with NPs with a CPT/CUR ratio of 4:1 showing the highest anticancer activity toward Colon-26 cells. These studies unambiguously demonstrate that dual-drug–loaded NPs act in a synergistic manner to effectively reduce the dose of drug required. In future, we envision expanding the utility of these NPs, particularly through conjugation of active targeting ligands, further improving their therapeutic efficacy.

Acknowledgements

This work was supported by grants from the Department of Veterans Affairs (Merit Award to D.M.), the National Institutes of Health of Diabetes and Digestive and Kidney by the grants RO1-DK-071594 (to D.M.), the American Heart Association Postdoctoral Fellowship Grant 13POST16400004 (to B.X.), National Natural Science Foundation of China (grant numbers: 51503172 and 81571807) and Fundamental Research Funds for the Central Universities (SWU114086 and XDJK2015C067). D.M. is a recipient of a Career Scientist Award from the Department of Veterans Affairs.

Notes and references

[a]*Institute for Clean Energy and Advanced Materials, Faculty for Materials and Energy, Southwest University, Chongqing, 400715, P. R. China*

[b]*Center for Diagnostics and Therapeutics, Institute for Biomedical Science, Georgia State University, Atlanta, 30302, USA. E-mail: bxiao@gsu.edu; Fax: +1-404-413-3580; Tel: +1-404-413-3597*

[c]*Atlanta Veterans Affairs Medical Center, Decatur, 30033, USA*

† Electronic supplementary information (ESI) available: UV-vis absorption and fluorescence spectra of free CPT and free CUR dissolved in DMSO. See DOI: 10.1039/b000000x/

1. C. Twelves, A. Wong, M. P. Nowacki, M. Abt, H. Burris, A. Carrato, J. Cassidy, A. Cervantes, J. Fagerberg, V. Georgoulias, F. Husseini, D. Jodrell, P. Koralewski, H. Kröning, J. Maroun, N. Marschner, J. McKendrick, M. Pawlicki, R. Rosso, J. Schüller, J. Seitz, B. Stabuc, J. Tujakowski, G. V. Hazel, J. Zaluski, W. Scheithauer, *N. Engl. J. Med.*, 2005, **352**, 2696.
2. J. Terzic, S. Grivennikov, E. Karin, M. Karin, *Gastroenterology*, 2010, **138**, 2101.
3. C. Liu, G. Zhao, J. Liu, N. Ma, P. Chivukula, L. Perelman, K. Okada, Z. Chen, D. Gough, L. Yu, *J. Control. Release*, 2009, **140**, 277.
4. S. J. Dylla, L. Beviglia, I. K. Park, C. Chartier, J. Raval, L. Ngan, K. Pickell, J. Aguilar, S. Lazetic, S. Smith-Berdan, M. F. Clarke, T. Hoey, J. Lewicki, A. L. Gurney, *PLoS One*, 2008, **3**, e2428.
5. M. Dean, T. Fojo, S. Bates, *Nat. Rev. Cancer*, 2005, **5**, 275.
6. W. Tian, J. Liu, Y. Guo, Y. Shen, D. Zhou, S. Guo, *J. Mater. Chem. B Mater. Biol. Med.*, 2015, **3**, 1204.
7. D. Lane, *Nat. Biotechnol.*, 2006, **24**, 163.
8. T. Ramasamy, J. H. Kim, J. Y. Choi, T. H. Tran, H. G. Choi, C. S. Yong, J. O. Kim, *J. Mater. Chem. B Mater. Biol.*, 2014, **2**, 6324.
9. J. Lehar, A. S. Krueger, W. Avery, A. M. Heibut, L. M. Johansen, E. R. Price, R. J. Rickles, G. F. Short III, J. E. Staunton, X. Jin, M. S. Lee, G. R. Zimmermann, A. A. Borisy, *Nat. Biotechnol.*, 2009, **27**, 659.
10. W. Ha, J. Yu, X. Y. Song, Z. J. Zhang, Y, Q, Liu, Y. P. Shi, *J. Mater. Chem. B Mater. Biol.*, 2013, **1**, 5532.
11. S. Aryal, C. M. J. Hu, L. F. Zhang, *Mol. Pharm.*, 2011, **8**, 1401.

12. K. H. Min, K. Park, Y. S. Kim, S. M. Bae, S. Lee, H. G. Jo, R. W. Park, I. S. Kim, S. Y. Jeong, K. Kim, I. C. Kwon, *J. Control. Release*, 2008, **127**, 208.
13. J. M. Covey, C. Jaxel, K. W. Kohn, Y. Pommier, *Cancer Res.*, 1989, **49**, 5016.
14. P. Darpa, C. Beardmore, L. F. Liu, *Cancer Res.*, 1990, **50**, 6919.
15. A. G. Cheetham, P. Zhang, Y. A. Lin, R. Lin, H. Cui, *J. Mater. Chem. B Mater. Biol.*, 2014, **2**, 7316.
16. W. Zhang, X. Y. Zhou, T. Liu, D. Ma, W. Xue, *J. Mater. Chem. B Mater. Biol.*, 2015, **3**, 2127.
17. W. Scarano, P. de Souza, M. H. Stenzel. *Biomater. Sci.*, 2015, **3**, 163.
18. P. Anand, A. B. Kunnumakkara, R. A. Newman, B. B. Aggarwal, *Mol. Pharm.* 2007, **4**, 807.
19. S. Prasad, S. C. Gupta, A. K. Tyagi, B. B. Aggarwal. *Biotechnol. Adv.*, 2014, **32**, 1053.
20. H. Cao, Y. Wang, X. He, Z. Zhang, Q. Yin, Y. Chen, H. Yu, Y. Huang, L. Chen, M. Xu, W. Gu, Y. Li. *Mol. Pharm.*, 2015, **12**, 922.
21. S. C. Gupta, S. Patchva, B. B. Aggarwal, *AAPS J.*, 2013, **15**, 195.
22. S. Ganta, M. Amiji, *Mol. Pharm.*, 2009, **6**, 928.
23. C. M. J. Hu, L. F. Zhang, *Biochem. Pharmacol.*, 2012, **83**, 1104.
24. C. M. J. Hu, S. Aryal, L. F. Zhang, *Ther. Deliv.*, 2010, **1**, 323.
25. M. Saraswathy, S. Q. Gong, *Mater. Today*, 2014, **17**, 298.
26. S. Aryal, C. M. J. Hu, L. F. Zhang, *Small*, 2010, **6**, 1442.
27. R. Misra, S. K. Sahoo, *Mol. Pharm.*, 2011, **8**, 852.
28. D. Zucker, Y. Barenholz, *J. Control. Release*, 2010, **146**, 326.
29. L. Cai, G. Xu, C. Shi, D. Guo, X. Wang, J. Luo. *Biomaterials*, 2015, **37**, 456.

30. B. Xiao, M. Zhang, E. Viennois, Y. Zhang, N. Wei, M. T. Baker, Y. Jung, D. Merlin, *Biomaterials*, 2015, **48**, 147.
31. S. Acharya, S. K. Sahoo, *Adv. Drug Deliv. Rev.*, 2011, **63**, 170.
32. X. Li, C. X. Gao, Y. P. Wu, C. Y. Cheng, W. Xia, Z. Zhang, *J. Mater. Chem. B Mater. Biol.*, 2015, **3**, 1556.
33. A. Verma, F. Stellacci, *Small*, 2010, **6**, 12.
34. K. Xiao, Y. Li, J. Luo, J. S. Lee, W. Xiao, A. M. Gonik, R. G. Agarwal, K. S. Lam, *Biomaterials*, 2011, **32**, 3435.
35. E. Frohlich, *Int. J. Nanomedicine*, 2012, **7**, 5577.
36. R. Yang, W. S. Shim, F. D. Cui, G. Cheng, X. Han, Q. Jin, D. Kim, S. Chung, C. Shim, *Int. J. Pharm.*, 2009, **371**, 142.
37. B. Xiao, H. Laroui, E. Viennois, S. Ayyadurai, M. A. Charania, Y. Zhang, Z. Zhang, M. T. Baker, B. Zhang, A. T. Gewirtz, D. Merlin, *Gastroenterology*, 2014, **146**, 1289.
38. B. Xiao, Y. Wan, M. Q. Zhao, Y. Q. Liu, S. M. Zhang, *Carbohyd. Polym.*, 2011, **83**, 144.
39. M. Lavertu, S. Methot, N. Tran-Khanh, M. D. Buschmann, *Biomaterials*, 2006, **27**, 4815.
40. M. E. I. Badawy, E. I. Rabea, *Postharvest Biol. Technol.*, 2009, **51**, 110.
41. E. Cohen-Sela, M. Chorny, N. Koroukhov, H. D. Danenberg, G. Golomb, *J. Control. Release*, 2009, **133**, 90.
42. C. E. Mora-Huertas, H. Fessi, A. Elaissari, *Adv. Colloid. Interface Sci.*, 2011, **163**, 90.
43. Y. F. Chen, Z. Rosenzweig, *Nano Lett.*, 2002, **2**, 1299.
44. L. Mu, S. S. Feng, *Pharm. Res.*, 2003, **20**, 1864.
45. C. M. Hassan, N. A. Peppas, *Adv. Polym. Sci.*, 2000, **153**, 37.
46. H. Chen, W. Yang, H. Chen, L. Liu, F. Gao, X. Yang, Q. Jiang, Q. Zhang, Y. Wang, *Colloids Surf. B*, 2009, **73**, 212.

47. Y. Wang, P. Li, L. Kong, *AAPS PharmSciTech*, 2013, **14**, 585.
48. H. Laroui, A. L. Theiss, Y. Yan, G. Dalmasso, H. T. T. Nguyen, S. V. Sitaraman, D. Merlin, *Biomaterials*, 2011, **32**, 1218.
49. A. M. Smith, H. Duan, A. M. Mohs, S. M. Nie, *Adv. Drug. Deliv. Rev.*, 2008, **60**, 1226.
50. T. H. Kim, J. E. Ihm, Y. J. Choi, J. W. Nah, C. S. Cho, *J. Control. Release*, 2003, **93**, 389.
51. Y. M. Liu, T. M. Reineke, *J. Am. Chem. Soc.*, 2005, **127**, 3004.
52. H. Wu, S. Wang, H. Fang, X. Zan, X. Zan, J. Zhang, Y. Wan, *Colloids Surf. B*, 2011, **82**, 602.
53. A. J. Souers, J. D. Leverson, E. R. Boghaert, S. L. Ackler, N. D. Catron, J. Chen, B. D. Dayton, H. Ding, S. H. Enschede, W. J. Fairbrother, D. C. Huang, S. G. Hymowitz, S. Jin, S. L. Khaw, P. J. Kovar, L. T. Lam, J. Lee, H. L. Maecker, K. C. Marsh, K. D. Mason, M. J. Mitten, P. M. Nimmer, A. Oleksijew, C. H. Park, C. M. Park, D. C. Phillips, A. W. Roberts, D. Sampath, J. F. Seymour, M. L. Smith, G. M. Sullivan, S. K. Tahir, C. Tse, W. D. Wendt, Y. Xiao, J. C. Xue, H. Zhang, R. A. Humerickhouse, S. H. Rosenberg, S. W. Elmore. *Nat. Med.*, 2013, **19**, 202.
54. B. Xiao, H. Laroui, S. Ayyadurai, E. Viennois, M. A. Charania, Y. Zhang, D. Merlin, *Biomaterials*, 2013, **34**, 7471.
55. G. Park, C. K. Choi, A. E. English, T. E. Sparer, *Cell Biol. Int.*, 2009, **33**, 429.

Figure captions

Figure 1. Preparation of cationic CPT/CUR-NPs using a one-step fabrication process. (a) Schematic illustration of the preparation of cationic CPT/CUR-NPs. Representative size distribution (b) and TEM image (c) of cationic CPT/CUR-NPs (4:1). Inset: TEM of an individual NP.

Figure 2. XRD patterns of free CPT (a), free CUR (b), and cationic CPT/CUR-NPs (4:1) (c).

Figure 3. *In vitro* cumulative release of CPT and CUR from cationic CPT/CUR-NPs (1:1) in PBS containing 0.5% Tween-80 at 37 ℃. Data are presented as means ± S.E.M. (n = 3).

Figure 4. Cellular colocalization of cationic CPT/CUR-NPs (1:1) in Colon-26 cells after treatment with a drug concentration of 100 μM for 3 h. Fluorescence images show the intracellular colocalization of CPT and CUR in Colon-26 cells. Scale bar = 10 μm.

Figure 5. Quantification of cellular uptake of various NPs by Colon-26 cells. (a) Representative flow cytometry histograms of fluorescence intensity for cells treated with free CPT or various NPs (CPT, 50 μM) for 3 h. (b) Percentage of CPT-containing Colon-26 cells after treatment with free CPT or NPs (CPT, 50 μM) for 3 h. (c) Representative flow cytometry plots of cells incubated with or without cationic CPT/CUR-NPs (1:1) for 3 h. Each point represents the mean ± S.E.M. (n = 3; $*P < 0.05$ and $**P < 0.01$, Student's *t*-test).

Figure 6. *In vitro* cytotoxicity of free drugs and various NPs against Colon-26 cells, determined by MTT assays. (a) Cytotoxicity of different concentrations of empty cationic NPs towards Colon-26 cells after incubation for 24 and 48 h. Cytotoxicity of free drugs and various NPs at different concentrations towards Colon-26 cells after incubation for 24 h (b) and 48 h (c). (d) Cytotoxicity of various cationic CPT/CUR-NPs with different weight ratios after incubation for 24 and 48 h. Triton X-100 (0.1%) was used as a positive control to produce a maximum cell death rate (100%); cell culture medium was used as a negative

control (death rate defined as 0%). Cytotoxicity is given as the percentage of viable cells remaining after treatment. Each point represents the mean ± S.E.M. (n = 5).

Figure 7. CI versus F_a plot. Colon-26 cells were incubated with various cationic CPT/CUR NPs for 24 h (a) and 48 h (b).

Figure 8. *In vitro* inhibition of the expression of Bcl-2 gene in Colon-26 cells (a). Cells were treated with different NPs (total drugs: 25 μM) for 8 h. Each point represents the mean ± S.E.M. (n = 3; $*P < 0.05$ and $**P < 0.01$, Student's *t*-test). The real-time cytotoxicity of various NPs against Caco2-BBE cells (b), determined using ECIS technology. ECIS was used to determine cell viability in real time during an extended exposure to an NP suspension with a drug concentration of 25 μM. As controls, ECIS was also performed on untreated cells and cells treated with Triton X-100 (0.5%) in DMEM.

1 **Fig. 1**

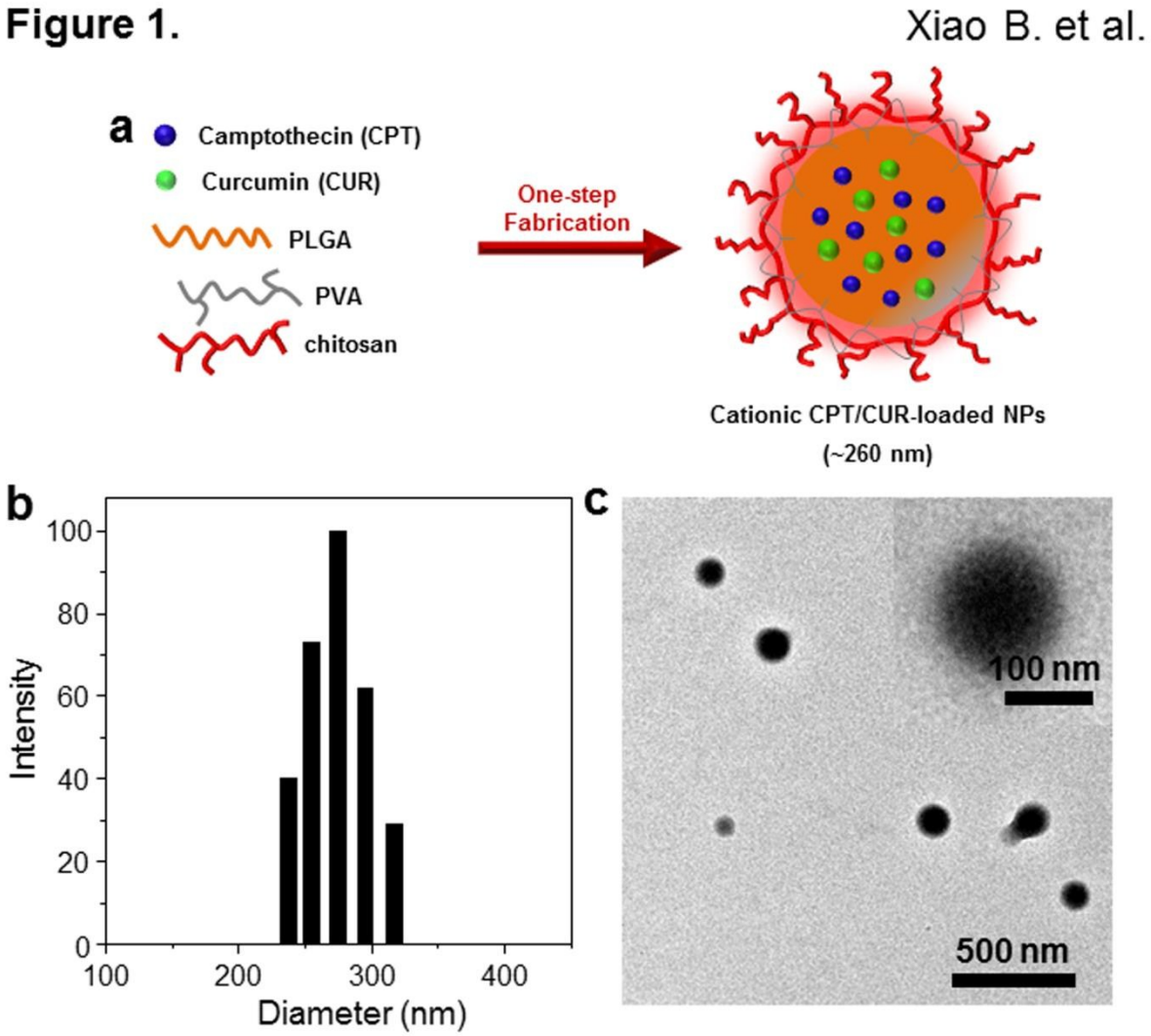

2

1 **Fig. 2**

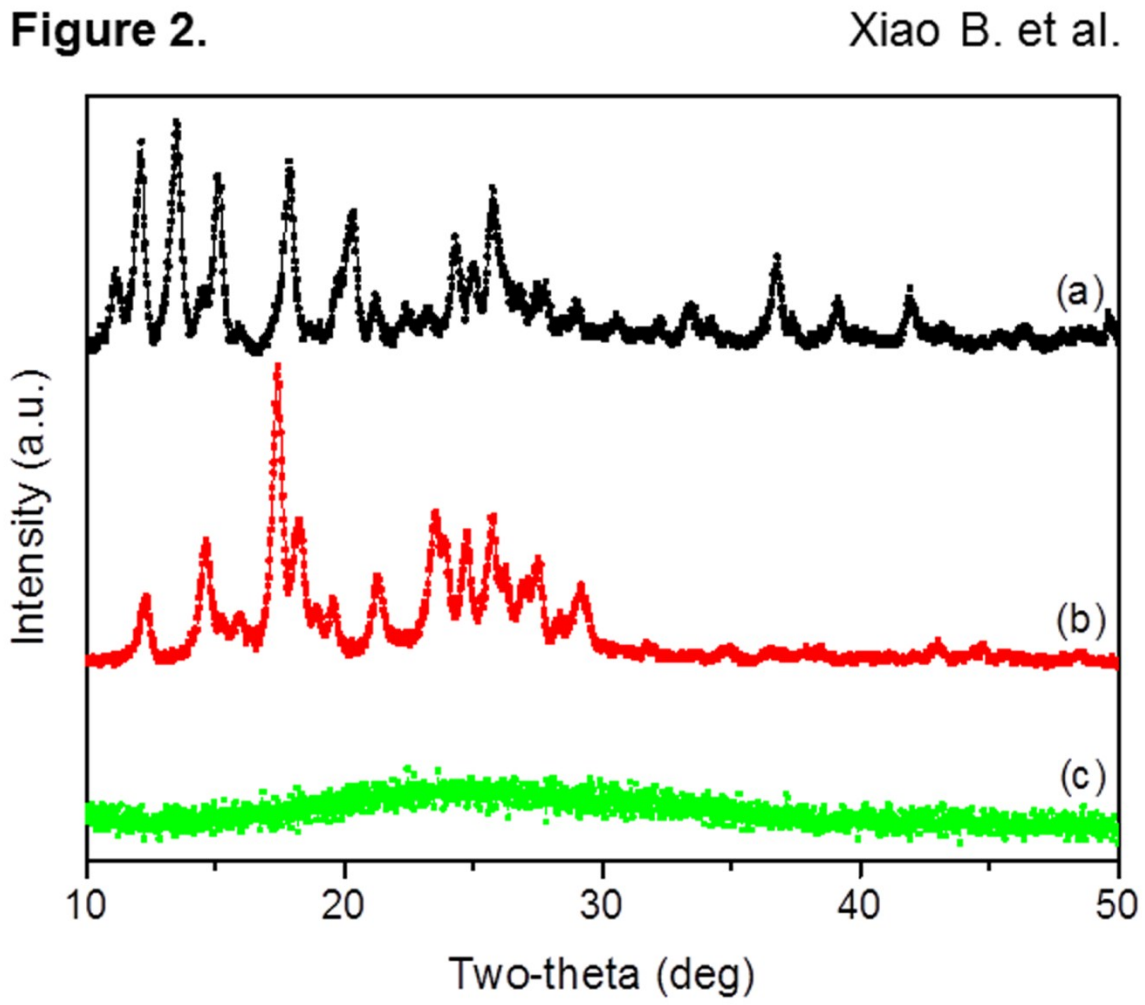

2

1 **Fig. 3**

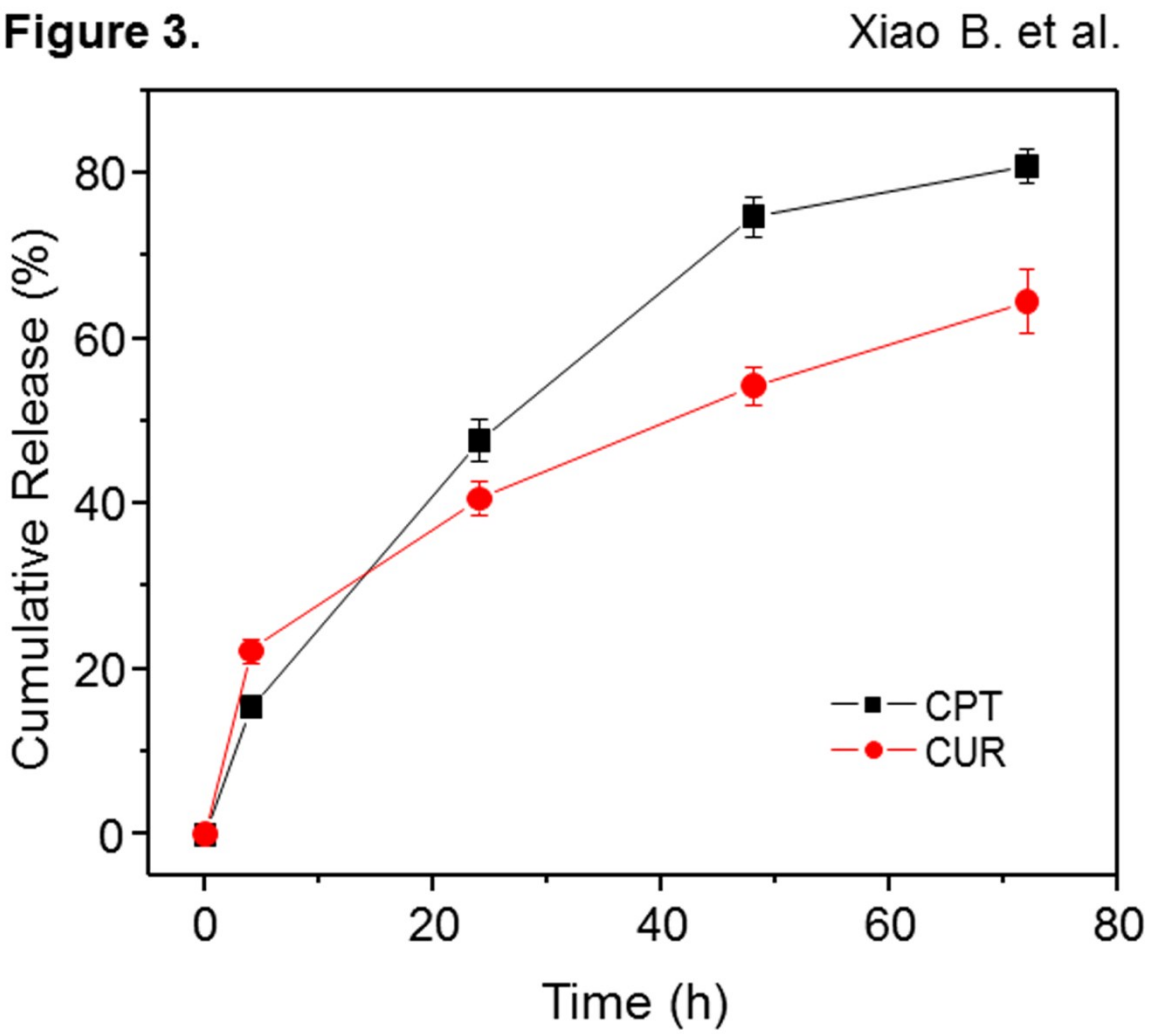

2

1 **Fig. 4**

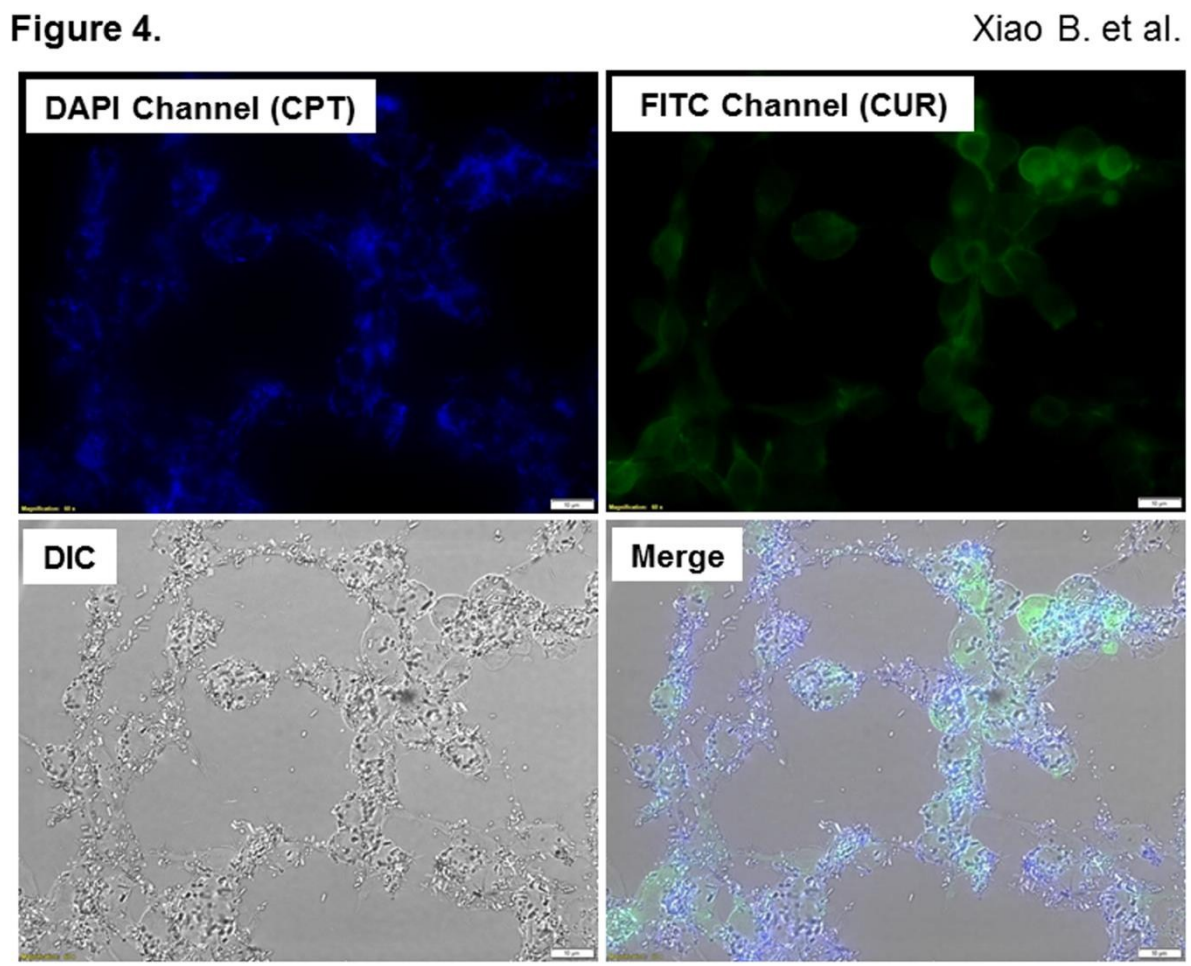

2

1 **Fig. 5**

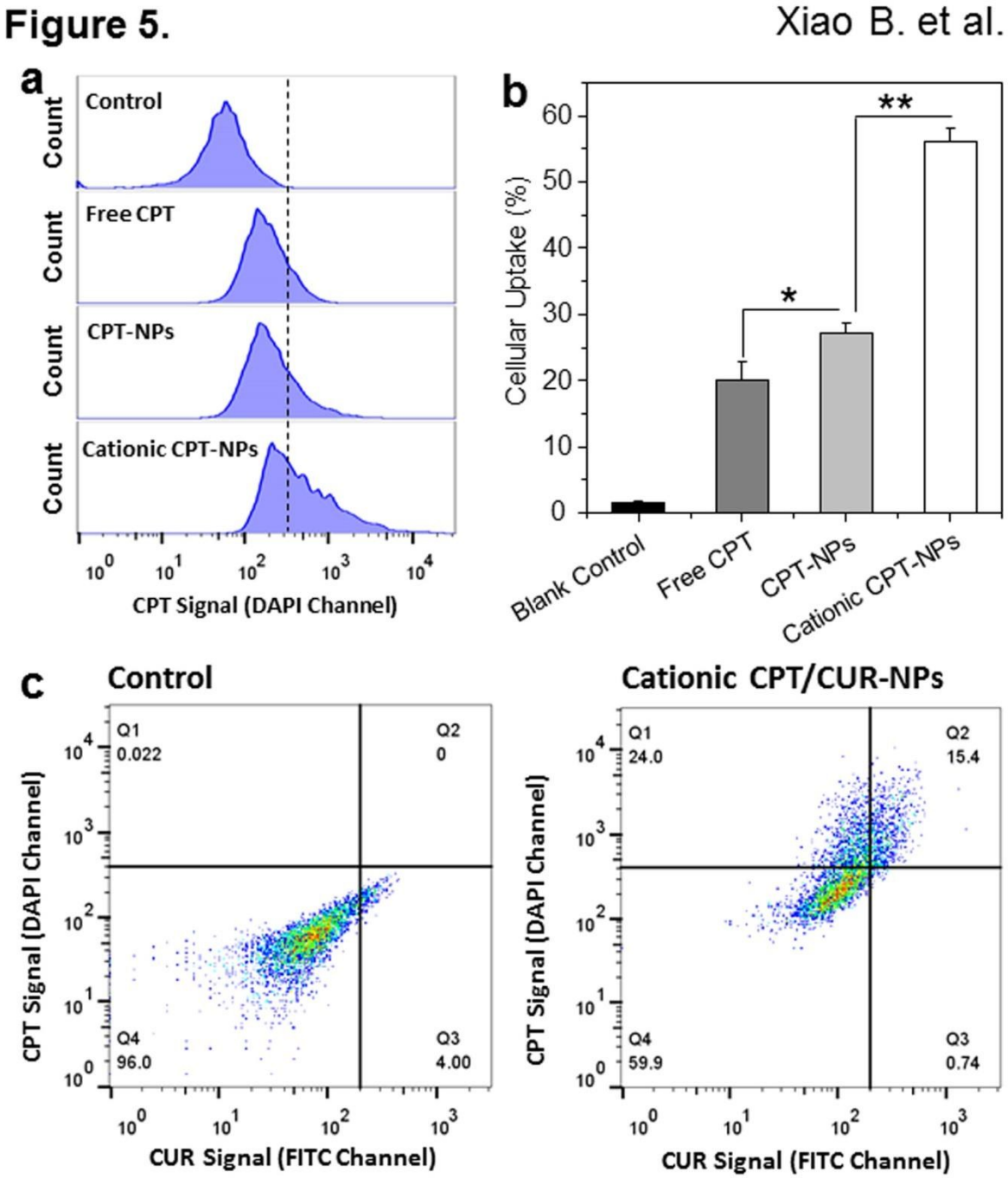

2

3

1 **Fig. 6**

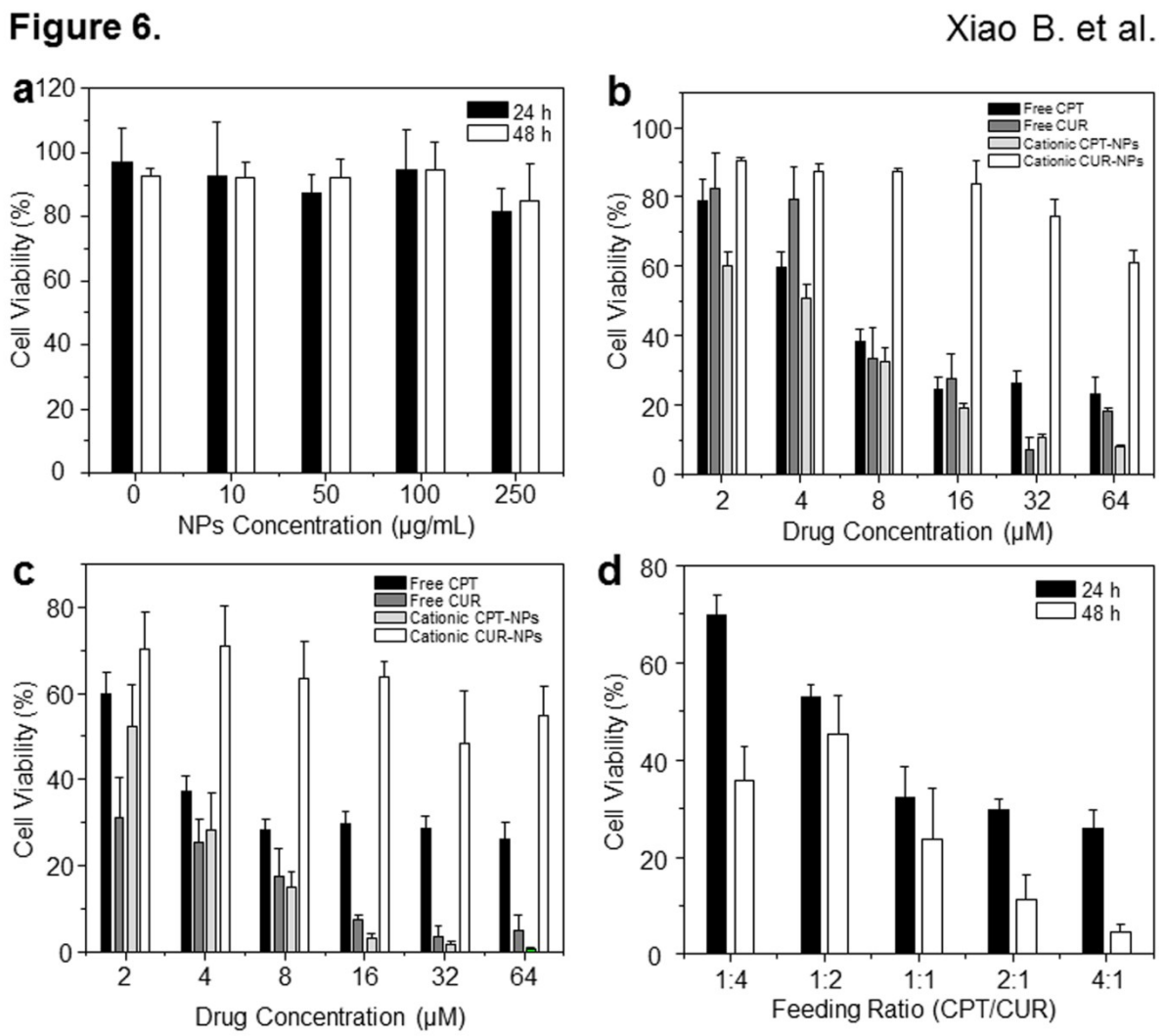

2

3

1 **Fig. 7**

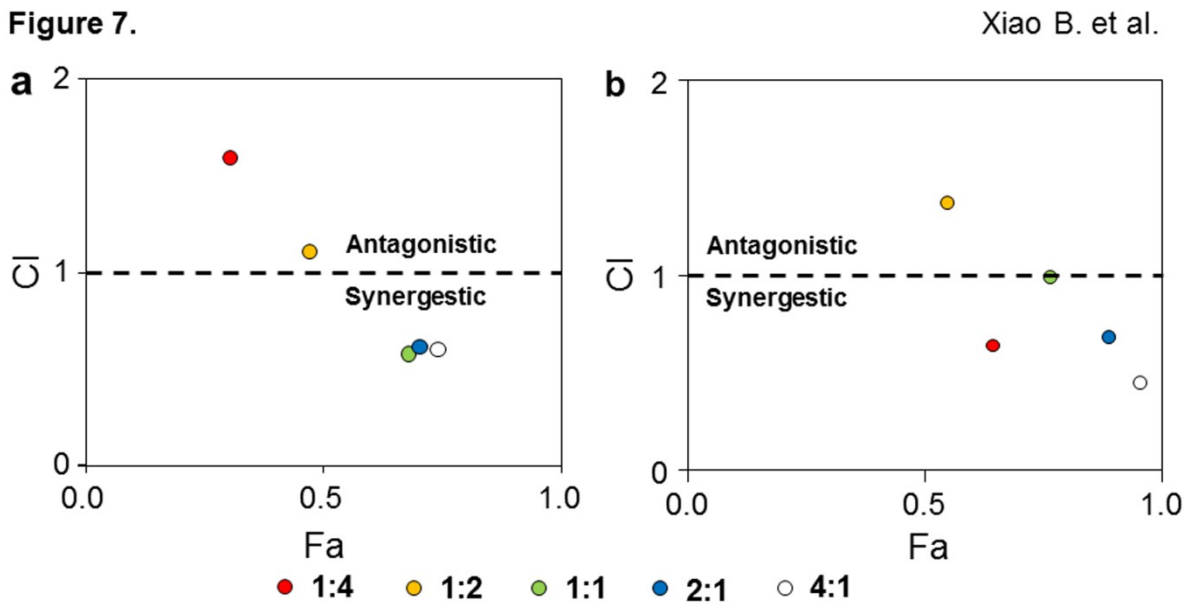

2

3

1 **Fig.8**

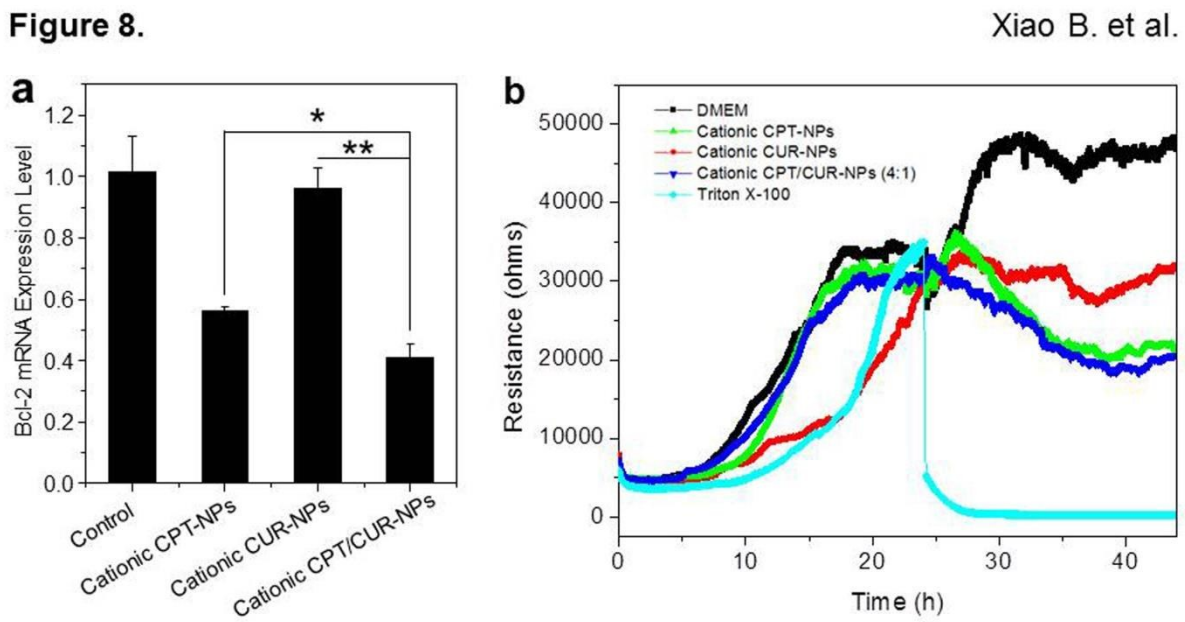

2

3

Table 1

Characteristics of the various nanoparticles (mean ± S.E.M.; n=3).

Nanoparticles	Particle Size (nm)	Zeta-potential (mV)	Drug Loading (%)		Encapsulation Efficiency (%)	
			CPT	CUR	CPT	CUR
Cationic Blank NPs	248.9 ± 7.4	+12.0 ± 2.9	–	–	–	–
CPT-NPs	240.8 ± 13.9	-12.6 ± 2.9	5.8 ± 0.4	–	96.8 ± 4.2	–
Cationic CPT-NPs	233.4 ± 7.9	+26.3 ± 2.5	5.1 ± 0.3	–	86.0 ± 3.2	–
Cationic CUR-NPs	243.1 ± 12.2	+19.3 ± 2.6	–	2.9 ± 0.2	–	48.8 ± 2.0
Cationic CPT/CUR-NPs (1:4)	204.9 ± 8.4	+19.2 ± 2.6	0.6 ± 0.2	1.7 ± 0.1	39.8 ± 2.8	35.4 ± 1.7
Cationic CPT/CUR-NPs (1:2)	193.0 ± 5.0	+28.1 ± 2.2	1.1 ± 0.3	1.6 ± 0.2	45.1 ± 3.4	39.3 ± 2.2
Cationic CPT/CUR-NPs (1:1)	204.3 ± 11.0	+14.6 ± 2.1	1.2 ± 0.2	0.9 ± 0.1	38.0 ± 4.1	35.7 ± 1.1
Cationic CPT/CUR-NPs (2:1)	224.6 ± 10.6	+ 20.4 ± 2.1	1.8 ± 0.2	0.8 ± 0.2	48.7 ± 3.2	44.8 ± 4.5
Cationic CPT/CUR-NPs (4:1)	209.2 ± 15.9	+12.2 ± 4.7	2.8 ± 0.3	0.5 ± 0.1	51.3 ± 4.8	39.5 ± 3.8

Table 2

IC_{50} (μM) of free drug and drug-loaded nanoparticles against Colon-26 cells line.

Incubation time	Free CPT	Free CUR	Cationic CPT-NPs	Cationic CUR-NPs
24 h	6.9	7.5	3.5	270.6
48 h	1.7	0.8	2.2	81.1

Table 3

Primers used in this study.

Primer name	Sequence	Description
Bcl-2-F	5'-GTACCTGAACCGGCATCTG-3'	Bcl-2 gene RT-PCR forward primer
Bcl-2-R	5'-GGGGCCATATAGTTCCACAA-3'	Bcl-2 gene RT-PCR reverse primer
36B4-F	5'-TCCAGGCTTTGGGCATCA-3'	36B4 gene RT-PCR forward primer
36B4-R	5'-CTTTATCAGCTGCACATCACTCAGA-3'	36B4 gene RT-PCR reverse primer

Graphical Abstract:

Camptothecin (CPT) and curcumin (CUR) have been co-loaded into cationic polymeric nanoparticles and exhibited strong synergistic effects against colon cancer cells.